Stable Jet Modes: A Special Case of Eddy and Mean Flow Interaction

JAMES C. MCWILLIAMS

National Center for Atmospheric Research[1], Boulder, Colo. 80307

(Manuscript received 20 June 1977, in final form 28 November 1977)

ABSTRACT

The quasi-geostrophic, small-amplitude free modes of oscillation are examined for a midlatitude ocean basin with mean currents. Attention is restricted to a particular class of mean currents which are solutions of nonlinear, inviscid and unforced equations and whose free modes are all stable ones. Among the free modes are ones confined to the narrow regions where the mean jets are strongest. These modes, dubbed "jet modes", have the following properties: 1) their phase speed is in the direction of and of the order of magnitude of the mean jet maximum velocity; 2) they are vertically in phase and upper-layer intensified when the mean jet is upper-layer intensified in phase and the thermocline is shallow; 3) they have a broader horizontal scale in the deep water than in the thermocline; 4) they have horizontal critical layers whose local balance is a nonlinear rather than a frictional one; 5) their Doppler-shifted frequencies are proportional to a mean potential vorticity gradient dominated by the horizontal curvature of the mean jet; 6) and their mean energy and potential vorticity flux divergences are small or—in the particular geometry of a channel—zero. It is argued that many of these features should characterize the transience of narrow jets in general, especially those features relating to the spatial structure of the modes. (The stability and dispersion relation characteristics should be more peculiar to the type of jet present.)

1. Introduction

There are many aspects to the interrelation between mean flows (or at least flows with very long time scales) and more rapidly varying fluctuations about them, i.e., eddies. A frequent concern in studies of this interrelation has been with systematic transfers of energy between the two types of currents. If the transfer is from mean to eddy, the process is referred to as an instability; in the reverse direction, the divergences of eddy momentum and buoyancy fluxes can generate mean currents. There is another aspect of this interrelation, however, which less obviously involves transfer: the presence of a strong mean flow can impose important structural constraints upon the eddies, even in the absence of an instability. An archetype for this process, consistent with the restrictions of quasi-geostrophic dynamics, is described below and will be referred to as a jet mode. It will be argued that the jet mode can serve as an idealization for ocean transience which might be useful, as the familiar barotropic and baroclinic modes [appropriate to a resting, flat-bottom ocean (see Veronis and Stommel, 1956)] and topographic modes [appropriate to a resting ocean over a linear bottom slope (see Rhines, 1970)] have proved to be, even in the complicated circumstances which actually occur.

Unfortunately, the jet modes are not simply solved for. However, this should not impair their value as archetypes, if their characteristics prove to be ones which occur for general narrow-jet structures.

2. Mean flow and linearized waves

In this section we shall derive nondimensional equations for mean currents and linearized perturbations about them within an enclosed ocean basin. For two immiscible fluid layers of slightly different densities, in a rotating reference frame, in hydrostatic balance and without forcing or dissipation, the dimensional momentum and mass balances in each layer are

$$\left.\begin{aligned}(\partial/\partial t + \mathbf{u}_i'\cdot\nabla)\mathbf{u}_i' + \mathbf{f}'\times\mathbf{u}_i' + g\nabla\eta_i' &= 0\\ (\partial/\partial t + \mathbf{u}_i'\cdot\nabla)h_i' + h_i'\nabla\cdot\mathbf{u}_i' &= 0\end{aligned}\right\}, \quad (1)$$

for $i = 1, 2$. The vector $\mathbf{f}'$ is the local vertical projection of the earth's rotation vector, $\mathbf{u}_i'$ the horizontal velocity in layer i, η_i' the corresponding pressure head, h_i' the thickness of that layer, and g the gravitational acceleration constant. The layer thicknesses may be written as

$$\left.\begin{aligned}h_1' &= h_0 + \Delta^{-1}[\eta_1'(1+\Delta) - \eta_2']\\ h_2' &= H_0 + \Delta^{-1}(\eta_2' - \eta_1') - B'\end{aligned}\right\}, \quad (2)$$

where h_0 and H_0 are the average layer thicknesses, Δ the positive relative density difference

[1] The National Center for Atmospheric Research is sponsored by the National Science Foundation.

0022-3670/78/0344-0362$09.50

between the layers, and $B'(x,y)$ the elevation of the bottom above its average level. An upper free surface condition has been assumed in writing (2); this yields the additional $O(\Delta)$ term in h_1' relative to what would result from a rigid lid condition (for currents on the scale of the internal radius of deformation).

Eqs. (1) and (2) are made nondimensional by the following scales:

$$\left.\begin{aligned} x,y &\sim L & \mathbf{f}' &\sim f_0 \\ h_2' &\sim H_0 & \mathbf{u}' &\sim V_0 \\ \eta_i' &\sim V_0 f_0 L/g & B' &\sim B_0 \\ t &\sim L/V_0 & h_1' &\sim h_0 \end{aligned}\right\}. \tag{3}$$

From these we obtain

$$\left.\begin{aligned} &R(\partial/\partial t + \mathbf{u}_i\cdot\nabla)\mathbf{u}_i + \mathbf{f}\times\mathbf{u}_i + \nabla\eta_i = 0 \\ &(\partial/\partial t + \mathbf{u}_i\cdot\nabla)h_i + h_i\nabla\cdot\mathbf{u}_i = 0 \end{aligned}\right\}, i = 1, 2 \\ \left.\begin{aligned} h_1 &= 1 + R\Gamma[\eta_1(1+\Delta) - \eta_2] \\ h_2 &= 1 + \delta R\Gamma(\eta_2 - \eta_1) - \sigma B \\ \mathbf{f} &= \hat{e}_z[1 + \beta(y - y_0)] \end{aligned}\right\}, \tag{4}$$

where the deletion of primes denotes nondimensional dependent variables, and the several nondimensional parameters are

$$\left.\begin{aligned} R &= V_0/f_0 L & \Gamma &= f_0^2 L^2/\Delta g h_0 \\ \delta &= h_0/H_0 & \sigma &= B_0/H_0 \\ \beta &= (\partial f'/\partial y')_0 L/f_0 \end{aligned}\right\}. \tag{5}$$

Respectively, these are an advective Rossby number, a Froude number, a ratio of layer thicknesses, a topographic Rossby number and a planetary Rossby number.

a. Mean flow

For steady motions ($\partial/\partial t = 0$), the mass conservation relations imply the existence of transport streamfunctions in each layer, i.e.,

$$h_i\mathbf{u}_i \equiv \hat{\mathbf{e}}_z \times \nabla\psi_i. \tag{6}$$

Furthermore, the equations in (4) may be manipulated to demonstrate the conservation of potential vorticity P_i and the Bernoulli function Q_i in each layer,

$$J(\psi_i, P_i) = J(\psi_i, Q_i) = 0, \tag{7}$$

where

$$\left.\begin{aligned} P_i &= h_i^{-1}\{f + R\nabla\cdot(\nabla\psi_i/h_i)\} \\ Q_i &= \eta_i + R\nabla\psi_i\cdot\nabla\psi_i/2h_i^2 \end{aligned}\right\}. \tag{8}$$

General integrals of (7), therefore, are P_i and Q_i being functions only of ψ_i; in this case, one may also derive from (4) the restriction that

$$P_i(\psi_i) = \frac{d}{d\psi_i} Q_i(\psi_i). \tag{9}$$

The mean flows which we shall consider will be obtained as solutions of (8) and (9). They represent baroclinic generalizations of those of Fofonoff (1954). It has been shown elsewhere (McWilliams, 1977a) that sufficient conditions for the stability of these mean solutions to infinitesimal perturbations (within enclosed domains on whose walls normal velocities must vanish) are the inequalities

$$\left.\begin{aligned} &h_i[\partial P_i(\psi_i)/\partial\psi_i] > 0 \\ &\tfrac{1}{2} \geqslant (R^2/h_i^3)\Gamma\nabla\psi_i\cdot\nabla\psi_i \times \begin{cases} 1 (i = 1) \\ \text{or} \\ \delta (i = 2) \end{cases} \end{aligned}\right\} \tag{10}$$

everywhere in the domain. For values of i corresponding to layers where $\psi_i \equiv 0$, we may disregard these conditions. The second of the relations in (10) is not a serious restriction on flows which have the parameters of midlatitude ocean gyres, and the first relation limits the class of $P(\psi)$ functionals for which stability is assured.

A particularly simple example of a stable solution to (8)–(9) is a linear potential vorticity function for flow confined to the upper layer only. In this case, we write

$$\left.\begin{aligned} P_1(\psi_1) &= a\psi_1 + b \\ Q_1(\psi_1) &= \tfrac{1}{2}a\psi_1^2 + b\psi_1 + c \\ h_1 &= 1 + R\Gamma(1+\Delta)\eta_1 \\ h_2 &= 1 - \sigma B - [\delta/(1+\Delta)](h_1 - 1) \end{aligned}\right\}, \tag{11}$$

and must solve the following coupled pair of equations for ψ_1 and η_1:

$$\left.\begin{aligned} &f + R\nabla\cdot(\nabla\psi_1/h_1) = h_1(a\psi_1 + b) \\ &(R/2h_1^2)\nabla\psi_1\cdot\nabla\psi_1 + \eta_1 = \tfrac{1}{2}a\psi_1^2 + b\psi_1 + c \end{aligned}\right\}. \tag{12}$$

For $a > 0$ the first condition in (10) is assured. An analytic solution of (12) may be obtained by an expansion in R for certain simple geometries. Solutions are discussed below for a zonal channel (Section 2) and a square basin (Section 6).

b. Linearized waves

We seek solutions to (4) which are small-amplitude perturbations about the mean flow solutions described in Section 2a. We further assume that $R \ll 1$ (though we initially leave the magnitudes of β and $R\Gamma$ unspecified) so as to eliminate high-frequency fluctuations. In such a case, it is convenient to examine the potential vorticity equation [obtained by eliminating the divergence between the mass equation and the curl of the momentum equation in (4)]. If for the fluctuation fields we neglect the fluid accelerations compared to the Coriolis and pressure terms (consistent with $R \ll 1$), then the result in each layer is

$$\bar{h}_i \frac{\bar{D}}{D_i t}\left[\frac{1}{h_i}\nabla\cdot\left(\frac{1}{f}\nabla\zeta_i\right)\right] - \bar{h}_i\bar{P}_i\frac{\bar{D}}{D_i t}(\mathfrak{h}_i/\bar{h}_i) + \bar{h}_i/fJ(\zeta_i,\bar{P}_i/R) = 0, \quad (13)$$

where the overbars refer to mean flow quantities, the ζ_i are the perturbation pressure heads and the $\mathfrak{h}_i$ are the perturbation thickness changes

$$\mathfrak{h}_1 = \Gamma[\zeta_1(1+\Delta) - \zeta_2], \quad \mathfrak{h}_2 = \delta\Gamma(\zeta_2 - \zeta_1). \quad (14)$$

We shall restrict our attention to perturbation solutions which are oscillatory in time; that is, we seek eigenfrequencies ω and eigenmodes $\zeta_i(x,y)e^{-i\omega t}$ for the pressure heads. In this case, the advective operator in (13) is

$$\frac{D}{D_i t} = [-i\omega + 1/\bar{h}_i J(\bar{\psi}_i, \ )]. \quad (15)$$

If we make the further restrictions that β and $R\Gamma$ are $\ll 1$, then in (13) $\bar{h}_i$ and f can be commuted with the advective operators and the functions f, $\bar{h}_i$ and $\bar{P}_i$ can be set to their constant, average values where they appear undifferentiated. Consistent with this, we could also set $\Delta = 0$ in (14). Eq. (13) applies whether there is a mean flow in layer i or not; when there is upper layer mean flow only, then, in addition to (11) and (12), we have

$$\left.\begin{aligned}\bar{P}_2 &= f/\bar{h}_2\\ \frac{\bar{D}}{D_2 t} &= -i\omega\end{aligned}\right\}. \quad (16)$$

To complete the statement of the eigenvalue problem associated with (13) and (14), we require boundary conditions on the ζ_i. No normal flow through the side boundary implies, by geostrophy, that on the wall

$$\zeta_i = C_i(t) = c_i e^{-i\omega t} \quad (17)$$

for each layer, where the c_i are numerical constants. As can be demonstrated by arguments analogous to those presented in McWilliams (1977b), a correct specification of the boundary constants is given by

$$\Delta\iint dxdy\zeta_1 = 0,^2 \quad \iint dxdy(\zeta_1 - \zeta_2) = 0. \quad (18)$$

c. Eddy fluxes

In this section we record the eddy flux divergences and forcing of the mean flow for linearized eigenmodes. If we were to partition the flow into mean and eddy components, then on the right-hand side of a momentum equation as in (4) would appear the term

$$-RM \equiv -R\overline{(\hat{\mathbf{u}}_i\cdot\nabla)\hat{\mathbf{u}}_i}, \quad (19)$$

where the caret refers to an eddy quantity and the overbar will be identified with a temporal average over an oscillation. For an expansion in R and small-amplitude eigenmode perturbations,

$$\boldsymbol{M}_i = \hat{\mathbf{e}}_z \times 2\,\mathrm{Re}[f^{-1}J(\zeta_i, f^{-1}\nabla\zeta_i^*)], \quad (20)$$

where the asterisk denotes complex conjugation. On the right-hand sides of mass conservation equations [as in (4)] would appear an eddy mass-flux divergence

$$-R\mathscr{H}_i \equiv -\overline{\nabla\cdot(\hat{h}_i\hat{\mathbf{u}}_i)} = -2R\Gamma\,\mathrm{Re}\left[J\left(\zeta_1^*, \frac{\zeta_1 - \zeta_2}{f}\right)\right], \quad -2R\delta\Gamma\,\mathrm{Re}\left[J\left(\zeta_2^*, \frac{\zeta_2 - \zeta_1}{f}\right)\right], \quad i = 1, 2. \quad (21)$$

These quantities must, of course, also appear as forcing terms in the mean depth-integrated energy equation or the mean potential vorticity equations for each layer. The manners in which they do so are as follows:

$$\tfrac{1}{2}(\partial/\partial t)\{\delta\bar{h}_1\bar{\mathbf{u}}_1^2 + \bar{h}_2\bar{\mathbf{u}}_2^2 + \Delta\delta\Gamma\bar{\eta}_1^2 + \delta\Gamma(\bar{\eta}_1 - \bar{\eta}_2)^2\} + \cdots = -\delta\bar{h}_1\bar{\mathbf{u}}_1\cdot\boldsymbol{M}_1 - \bar{h}_2\bar{\mathbf{u}}_2\cdot\boldsymbol{M}_2 - \delta(\bar{\eta}_1 + \tfrac{1}{2}R\bar{\mathbf{u}}_1^2)\times\mathscr{H}_1 - (\bar{\eta}_2 + \tfrac{1}{2}R\bar{\mathbf{u}}_2^2)\mathscr{H}_2$$

$$\bar{h}_i(\partial/\partial t)\bar{P}_i + \cdots = -R[\mathrm{curl}\boldsymbol{M}_i - \bar{P}_i\mathscr{H}_i], \quad (22)$$

where the dots appear in place of mean flow flux divergences.

3. Channel flow

A particularly simple example of the system discussed in Section 1 arises in a zonally oriented channel, where the mean flow is independent of the zonal coordinate and the eddies are zonally periodic.

If we restrict our attention to the mean flow defined by Eqs. (11) and (12), then we seek solutions $\bar{\psi}_1(y)$ and $\bar{h}_1(y)$. If R, $R\Gamma$, Δ and β are all small parameters, then a leading order solution will be

$$\left.\begin{aligned}\bar{\psi}_1(y) &= \beta/a(y - \sinh Qy/\sinh Q)\\ \bar{h}_1(y) &= 1 + R\Gamma[c + \bar{\psi}_1(y)]\end{aligned}\right\}, \quad (23)$$

where $Q = (a/R)^{1/2}$ and the domain in y is between 0 and 1 [with $y_0 = 0.5$ in the Coriolis function in (4)]. Because Q is a large number, the solution has a boundary layer; the constant b from (11) has been chosen equal to $1 - \beta/2$ so that the only boundary layer is on the northern wall, $y = 1$. This layer has an eastward jet (for $a > 0$), and the interior region

[2] When $\Delta = 0$, the first condition loses force and there exists a dynamically irrelevant arbitrariness, which, for example, can be removed by eliminating the barotropic mode on the walls (i.e., $\delta c_1 + c_2 = 0$). This specification is the one used in Section 6.

is one of slow westward return flow. There is no net transport across any meridian because of the boundary conditions $\psi_1 = 0$ at $y = 0$ and 1.[3]

The eigenvalue problem (13)–(18) also reduces to one spatial dimension. If we assume that the eigenmodes have a zonal dependence as e^{ikx}, then the differential equations (13) become

$$\left.\begin{aligned}[\bar{u}_1(y) - c][\zeta_{1,yy} - (k^2 + \Gamma)\zeta_1 + \Gamma\zeta_2] \\ + \mathscr{P}_1(y)\zeta_1 = 0 \\ c[\zeta_{2,yy} - (k^2 + \delta\Gamma)\zeta_2 + \delta\Gamma\zeta_1] - \mathscr{P}_2(y)\zeta_2 = 0\end{aligned}\right\}, \quad (24)$$

where $c = \omega/k$ and

$$\left.\begin{aligned}\bar{u}_1 &\equiv -\bar{\psi}_{1,y} = -\frac{\beta}{a}\left(Q\frac{\cosh Q_y}{\sinh Q} - 1\right), \\ \mathscr{P}_1 &\equiv \frac{1}{R}\bar{P}_{1,y} = -\frac{a}{R}\bar{u}_1 \\ \mathscr{P}_2 &\equiv \frac{1}{R}\bar{P}_{2,y} = \beta/R - \delta\Gamma\bar{u}_1\end{aligned}\right\}. \quad (25)$$

For analytical convenience we have made the additional assumption that the channel has a flat bottom [i.e., $\sigma = 0$ in Eq. (11)]. Because of the oscillatory zonal variations in a channel, the boundary conditions (18) here reduce to $\zeta_1 = \zeta_2 = 0$ on $y = 0$ and 1.

The middle formula in (25) has been evaluated using the first relation in (11). If we wished to examine the eigenmodes in a quiescent channel, then this relation would not be available to us (rather we should use $\bar{P}_1 = f$); in this case, we would set $\bar{u}_1$ to zero and insert $\mathscr{P}_1 = \mathscr{P}_2 = \beta/R$ in (24). The solutions then would be the familiar Rossby wave modes

$$\zeta_1 = \mu\zeta_2 = \sin m\pi y,$$

with

$$(c,\mu) = \begin{cases}[-\beta/R(k^2 + m^2\pi^2),\ 1] \\ [-\beta/R(k^2 + m^2\pi^2 + \Gamma(1 + \delta)),\ -1/\delta]\end{cases} \quad (26)$$

for the barotropic and baroclinic solutions, respectively. Heuristically, we might expect that, as $Q \to \infty$, there would be eigenmodes of (24) and (25) which have no important variation on the boundary layer scale $\Delta y = 1/Q$ even when $\bar{u}_1 \neq 0$. If we were to solve (24), arbitrarily neglecting those coefficients in the differential equation with this "fast" scale, then we would recover (26) since $a \gg R$. Clearly, it would only be those Rossby modes with small m and k values which might also be approximate solutions of (24). An example of an approximate Rossby mode is given in Section 6.

There is another class of eigenmodes, however, which are less familiar than the Rossby modes. They are ones whose existence is crucially dependent upon the mean boundary jet. To expose them we transform Eq. (24) to a boundary layer coordinate $\eta = Q(1 - y)$ and rescale the constants of the problem

$$\left.\begin{aligned}&[\hat{c} - \hat{u}(\eta)](\zeta_{1\eta\eta} - K\zeta_1 + \gamma\zeta_2) - \hat{\mathscr{P}}_1(\eta)\zeta_1 = 0 \\ &\hat{c}\{\zeta_{2\eta\eta} - [K - (1 - \delta)\gamma]\zeta_2 + \delta\gamma\zeta_1\} - \hat{\mathscr{P}}_2(\eta)\zeta_2 = 0 \\ &\zeta_1 = \zeta_2 = 0 \quad \text{at} \quad \eta = 0 \quad \text{and} \quad Q\end{aligned}\right\}, \quad (27)$$

where

$$\left.\begin{aligned}&\hat{c} = \frac{ac}{\beta Q}; \quad K = (k^2 + \Gamma)/Q^2; \quad \gamma = \Gamma/Q^2 \\ &\hat{u}_1(\eta) = [\cosh(Q - \eta)/\sinh Q - 1/Q] \\ &\hat{\mathscr{P}}_1(\eta) = -\hat{u}_1(\eta) \\ &\hat{\mathscr{P}}_2(\eta) = 1/Q - \delta\gamma\hat{u}_1(\eta)\end{aligned}\right\}. \quad (28)$$

For this scaling to be sensible, both K and γ must be O(1) or smaller; that is, the zonal perturbation scale and the internal deformation radius must not be small relative to the width of the mean jet.

In the following section, several approximate solutions to (27) and (28) will be discussed. In assessing these approximations it will be useful to refer to an integral of the upper layer differential equation. If we multiply the first equation in (27) by $\zeta_1/(\hat{c} - \hat{u}_1)$ and integrate in η, we obtain

$$\int_0^Q d\eta(\hat{c} - \hat{u}_1)^2\left\{\left[\frac{\partial}{\partial\eta}\left(\frac{\zeta_1}{\hat{c} - \hat{u}_1}\right)\right]^2 + K[\zeta_1/(\hat{c} - \hat{u}_1)]^2\right\}$$

$$= -(1/Q)\int_0^Q d\eta(\hat{c} - \hat{u}_1)[\zeta_1/(\hat{c} - \hat{u}_1)]^2$$

$$+ \gamma\int_0^Q d\eta\zeta_1\zeta_2 + (\hat{c} - \hat{u}_1)\zeta_1[\zeta_1/(\hat{c} - \hat{u}_1)]_\eta\Big|_0^Q, \quad (29)$$

where the last term can be shown to vanish for the boundary conditions of (27). A similar quadratic integral for the lower layer equation in (27) is

$$\int_0^Q d\eta\left\{(\zeta_{2\eta})^2 + \left[K - \gamma(1 - \delta) + \frac{1 + \delta\gamma}{\hat{c}Q}\right]\zeta_2^2\right\}$$

$$= \delta\gamma\left[\int_0^Q d\eta\zeta_1\zeta_2 + \frac{1}{\hat{c}}\int_0^Q d\eta\frac{\cosh(Q - \eta)}{\sinh Q}\zeta_2^2\right] + \zeta_2\zeta_{2\eta}\Big|_0^Q. \quad (30)$$

For solutions to (27) and (28) that have real values of $\hat{c}$, ζ_1 and ζ_2, the eddy flux divergences assume a particularly simple form, *viz.*,

[3] The quantities a and Q are perhaps unfamiliar in a mean gyre solution. Q, the inverse ratio of the boundary layer and basin widths, is also the ratio of the maximum velocity to the maximum $\bar{\psi}$ (the interior transport); a, the mean potential vorticity gradient with respect to streamfunction, is the ratio of β to the interior transport.

$$M_i = -2(K-\gamma)Q\frac{\partial}{\partial\eta}(\zeta_i^2)\hat{\mathbf{e}}_y, \quad \mathcal{H}_i = 0. \quad (31)$$

Furthermore, the eddy contributions are nil in the mean energy and potential vorticity equations (22).

4. Jet modes

In this section several approximate solutions to (27) will be described. They are obtained by a mixed numerical-analytical technique which requires that K, γ and $\hat{c}$ be order unity numbers; in practice, this restriction excludes the greater part of the eigenmode spectrum and retains only the jet modes.

The strongest simplification which can be made to the correct eigenvalue problem (27) involves the following assumptions: 1) $|\zeta_2| \ll |\zeta_1|$ almost everywhere so that the term proportional to ζ_2 may be neglected in the upper layer equation; 2) the far boundary at $\eta = Q$ be removed to $\eta = \infty$; 3) the mean velocity $\hat{u}_1$ be approximated by a simple exponential decay in η; and, similarly, 4) in $\hat{\mathcal{P}}_2(\eta)$ the planetary vorticity gradient $1/Q$ be neglected relative to the term proportional to mean jet velocity (which arises from a lower layer thickness gradient). Under these assumptions, the eigenvalue problem is only a second-order differential equation; *viz.*,

$$(\hat{c} - e^{-\eta})[\zeta_{1\eta\eta} - K\zeta_1] + e^{-\eta}\zeta_1 = 0;$$
$$\zeta_1(0) = 0; \ \zeta_1 \to 0 \quad \text{as} \quad \eta \to \infty. \quad (32)$$

The lower layer equation is then simply a forced boundary value problem for ζ_2, once the eigensolutions $\hat{c}$ and ζ_1 are known from (31). This problem is

$$\left.\begin{aligned} &\zeta_{2\eta\eta} - [K - (1-\delta)\gamma + (\delta\gamma/\hat{c})e^{-\eta}]\zeta_2 = -\delta\gamma\zeta_1 \\ &\zeta_2(0) = 0; \quad \zeta_2 \to 0 \quad \text{as} \quad \eta \to \infty \end{aligned}\right\}. \quad (33)$$

The simplified equation (32) is a particular example of an eigenmode equation for barotropic, parallel flow. This subject has been extensively studied (e.g., Drazin and Howard, 1966), most commonly with regard to the question of instability. In our case, the question has been answered negatively, since (32) was derived from the more general equation (13) with only stable modes. Furthermore, the more common treatments of parallel flow eigenmodes have usually assumed a bounded domain in y with a dimension comparable to the scale of the mean flow; it is only for strong, narrow jets in a broad domain [assumptions (2)–(4) above] that the particular characteristics of jet modes arise.

It is convenient to further transform the independent variable for (32) and (33) to $\xi = e^{-\eta}$; thus

$$\left.\begin{aligned} &(\hat{c} - \xi)(\xi\zeta_1'' + \zeta_1') + (1 + K - \hat{c}K/\xi)\zeta_1 = 0 \\ &\xi^2\zeta_2'' + \xi\zeta_2' + (\gamma(1-\delta) - K \\ &\qquad + \delta\gamma\xi/\hat{c})\zeta_2 = -\delta\gamma\zeta_1 \\ &\zeta_1 = \zeta_2 = 0 \quad \text{at} \quad \xi = 0 \quad \text{and} \quad 1 \end{aligned}\right\}. \quad (34)$$

TABLE 1. Eigenmodes of (34).

(K, γ, δ)	$\hat{c}$	$\zeta_{1\max}$	$\xi(\zeta_{1\max})$	$\zeta_{2\max}$	$\xi(\zeta_{2\max})$
(0.5, 0.25, 0.16)	0.46	0.29	0.32	0.013	0.14
(0.4, 0.25, 0.16)	0.60	0.37	0.39	0.020	0.12
(0.5, 0.45, 0.16)	0.46	0.29	0.32	0.034	0.10
(0.5, 0.25, 0.10)	0.46	0.29	0.32	0.008	0.12

I know of no closed-form solutions to these equations. Consequently, a numerical solution technique is required; it is essentially a shooting technique and is described in the Appendix. However, the upper equation has two singular points (at $\xi = 0$ and $\hat{c}$), and explicit expansions about these points are required to obtain a valid solution.[4]

An example of a solution to (34) is shown in Fig. 1. The particular parameters chosen were $K = 0.5$, $\gamma = 0.25$ and $\delta = 0.16$; the resulting eigenvalue was $\hat{c} = 0.46$, which confirms *a posteriori* the appropriateness of the scaling which led to Eq. (27). The phase speed is to the east, in the direction of the jet, and has a value between the maximum and minimum jet speeds. No other eigenvalues were found in the range $\hat{c} \in [-2, 3]$; however, the solution technique described in the Appendix is inadequate for small values of $\hat{c}$ where the two singularities are very close to each other [which would be the case for quiescent modes (26) with $K \sim O(1)$].

The critical layer behavior can be seen from the upper left panel in Fig. 1 [as well as from the local expansion, Eq. (A6)]. The eigenmode $\zeta_1(\xi)$ is smoothly varying across the layer, but has a logarithmically infinite first derivative there; consequently, the upper layer momentum flux divergence from (31) is also locally infinite (see the lower right panel of Fig. 1). The upper and lower layer pressures are vertically in phase, and the latter is only 3% of the former in the region of largest ζ_1 values. However, the maximum value for ζ_2 occurs at larger η than for ζ_1 and the decay is slower. In fact, as $\eta \to \infty$,

[4] The second of these singularities is usually referred to as a critical layer. In the Appendix, Eqs. (A6)–(A9) and (A17)–(A18) describe local solutions similar to the Tollmien solutions near a critical layer in a parallel shear flow. Furthermore, they are such that there is no phase shift across the critical layer. This is appropriate as a linearized, inviscid approximation to the true fluctuation equations when $\lambda = K'/V_0L\alpha^{3/2}$ is small (n.b., K' is the dimensional coefficient of horizontal eddy viscosity and α, a wave Strouhal number, is the ratio of fluctuation to mean velocity scales) as α and $K' \to 0$. In this case nonlinear effects are more important than viscous effects locally, and the analysis of Benny and Bergeron (1969) is appropriate, rather than that of Lin (1966). Were λ large and a phase shift required in the critical layer solutions, then the results of Lin (1966) can be used to show that no jet modes would exist (i.e., that there would be no neutral modes with $\hat{c}$ order 1 and positive).

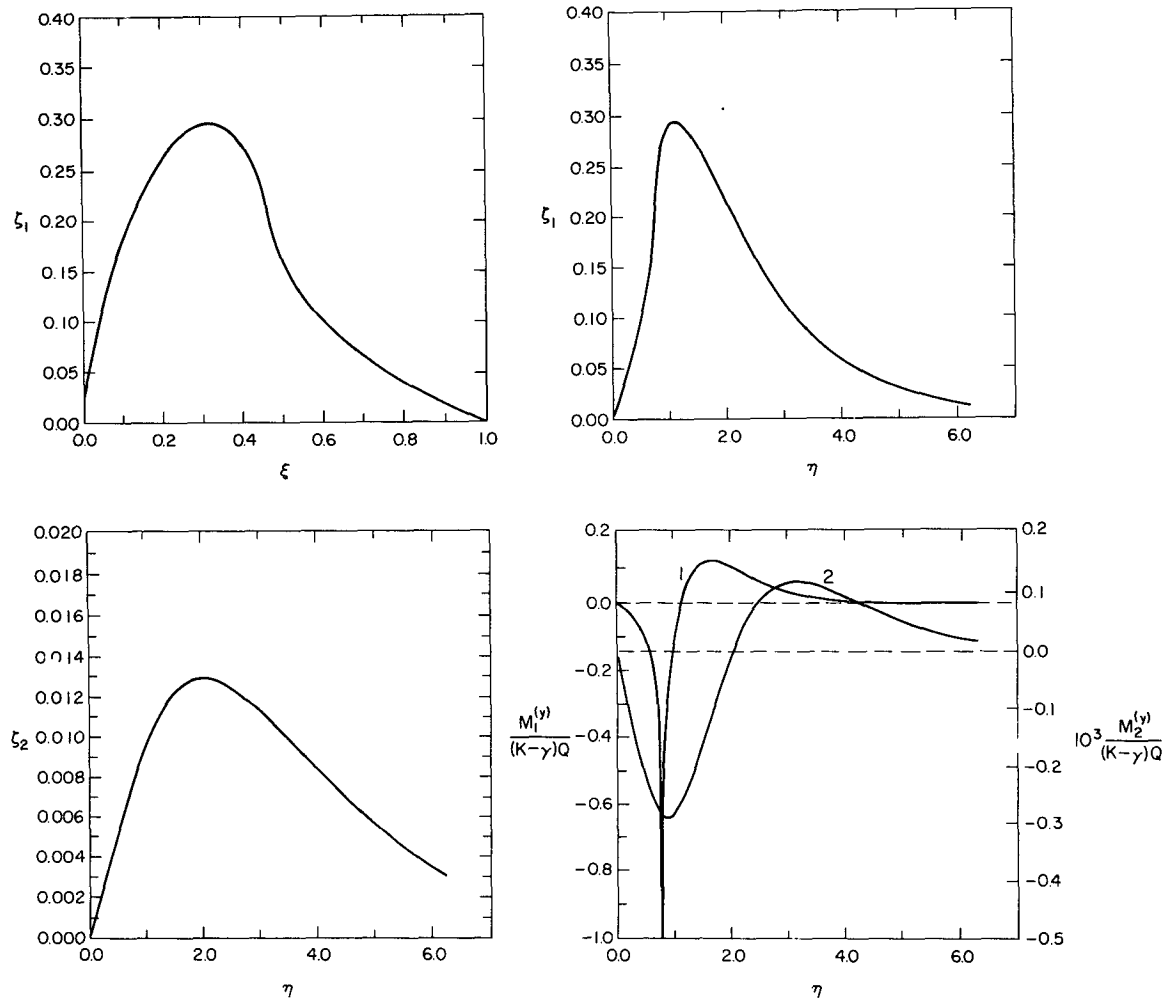

FIG. 1. A jet eigenmode from the approximate equations (34). The parameters selected were $K = 0.5$, $\gamma = 0.25$ and $\delta = 0.16$. The eigenvalue is $\hat{c} = 0.46$.

$$\left.\begin{aligned} \zeta_1 &\propto \exp(-K^{1/2}\eta) \\ \zeta_2 &\propto \exp\{-[K - \gamma(1-\delta)]^{1/2}\eta\} \end{aligned}\right\}. \tag{35}$$

The second exponential coefficient is a smaller positive number (for $\delta < 1$) than the first. The meridional momentum flux divergences in both layers have patterns which tend to accelerate a divergent mean flow (to the north in the northern part of the jet and to the south in the south) perpendicular to the jet axis. The cross-jet length scale of this pattern is larger in the lower layer than in the upper.

These characteristics also apply to other solutions of (34) for moderately different parameter values. Table 1 indicates parametric tendencies. The eigenmode problem depends only on K, and $\hat{c}$ varies inversely with it. As K increases, the maximum amplitude for ζ_1 decreases [relative to $Z(\xi = 0) = 1$, which is fixed by (A2)], and its location moves to smaller ξ (larger η) values. The lower layer pressure maximum decreases, however, and moves outward in ξ as K increases. As Γ increases, the ζ_2 maximum increases and moves inward in ξ; as δ increases, the ζ_2 maximum increases and its location varies little.

There appear to be no difficulties in obtaining solutions to (34) as K decreases from the values of Table 1. The eigenvalues $\hat{c}$ increase but remain well bounded by unity. On the other hand, solutions cannot be found for $K \gtrsim 0.56$. This failure is associated with $\hat{c}$ decreasing toward zero [and the singularities of (34) coalescing]. As remarked above, the techniques of Appendix A fail in such a case. However, it is clear from examining solutions as K approaches this cutoff from below that the largest values and gradient for ζ_1 are pushed towards small ξ values (large η values); thus, the solutions, even if they exist, are not properly to be considered jet modes in the sense defined by the transformation preceding Eq. (27).

The solutions of the type shown in Fig. 1 seem

self-consistent by the standards of the derivation of (34); however, they are inconsistent with a literal interpretation of the integral relation (29). Under the assumptions preceding Eq. (32), all of the right-hand side terms in (29) are absent; yet the left-hand side terms are all positive. The contradiction is not necessarily fatal: it is probable that the $\hat{c}$ eigenvalues and the $\zeta_1(\eta)$ solutions for order 1 values of η may be adequately approximated from (32), whereas the far field might not conform to the assumptions preceding (32) yet contribute substantially to (29). If we simply insert solutions such as are in Fig. 1 into the two right-hand side terms of (29), then the second is certainly positive—as required for balance—and so is the first if $\hat{c}$ is small enough. Nevertheless, the issue deserves further consideration.

We begin by examining the nature of the solutions to the exact problem (27) in the neighborhood of $\eta = Q$, where we can neglect $e^{-\eta}$ relative to $1/Q$ in (28). The solution which satisfies the boundary conditions as well as the differential equations is

$$\left.\begin{aligned}\zeta_1 &= 2A[\sinh\alpha(\eta - Q) + B\sinh\beta(\eta - Q)]\\ \zeta_2 &= 2A[(1/\mu_1)\sinh\alpha(\eta - Q)\\ &\qquad + (B/\mu_2)\sinh\beta(\eta - Q)]\end{aligned}\right\}, \quad (36)$$

where, in an expansion in $(\hat{c}Q)^{-1}$,

$$\left.\begin{aligned}\alpha^2 &= K + \delta\gamma + \frac{1+\delta+\gamma\delta^2}{1+\delta}\frac{1}{\hat{c}Q} + \ldots;\\ \frac{1}{\mu_1} &= -\delta - \frac{\delta^2}{1+\delta}\frac{1}{\hat{c}Q} + \ldots;\\ \beta^2 &= K - \gamma + \frac{1}{\hat{c}Q}\frac{1+2\delta}{1+\delta}\ldots;\\ \frac{1}{\mu_2} &= 1 - \frac{1}{\hat{c}Q}\frac{\delta}{1+\delta} + \ldots\end{aligned}\right\}. \quad (37)$$

The parameters A, B and $\hat{c}$ are undetermined here. The first can be identified with the indeterminate amplitude of an eigenvalue problem; the other two parameters are required to match (36) with the solution in the jet region [$\eta \sim O(1)$]. By comparing (36) with the $\eta \to \infty$ expansion (A4) for the approximate eigenmode from (32), we can see two major discrepancies: the exact solution has a decay rate α, while the previous ζ_1 had a decay rate $K^{1/2}$, and there is an entirely new component to (36), where $B \neq 0$, which is missing in (A4). Both of these errors were caused by the layer decoupling assumption preceding (32). For large $\hat{c}Q$ values, all of the other assumptions preceding (32) seem to have only minor consequences in (36). Therefore, as a minimal improvement of the previous approximation for jet modes, we can solve the following simplified version of (27):

$$\left.\begin{aligned}&(\hat{c} - e^{-\eta})[\zeta_{1\eta\eta} - K\zeta_1 + \gamma\zeta_2] - e^{-\eta}\zeta_1 = 0\\ &\zeta_{2\eta\eta} - \left[K - (1-\delta)\gamma + \frac{\delta\gamma}{\hat{c}}e^{-\eta}\right]\zeta_2 + \delta\gamma\zeta_1 = 0\\ &\zeta_1(0) = \zeta_2(0) \quad \text{at} \quad \eta = 0,\\ &\left.\begin{aligned}\zeta_1(\eta) &\approx \exp[-(K+\delta\gamma)^{1/2}\eta]\\ &+ B\exp[-(K-\gamma)^{1/2}\eta] + \ldots\end{aligned}\right\}\\ &\left.\begin{aligned}\zeta_2(\eta) &\approx -\delta\exp[-(K+\delta\gamma)^{1/2}\eta]\\ &+ B\exp[-(K-\gamma)^{1/2}\eta] + \ldots\end{aligned}\right\}\ \text{as}\ \ \eta\to\infty\end{aligned}\right\}. \quad (38)$$

The asymptotic decay in (38) has been derived from (36) and (37), and may be compared with (35). The solution technique for (38) is also described in the Appendix; it is a similar shooting method, except that now there are two eigenparameters to be determined—$\hat{c}$ and B.

A solution to the more accurate eigenvalue problem (38), which corresponds to the one shown in Fig. 1, is shown in Fig. 2. On the whole the two solutions are quite similar: the eigenvalue $\hat{c}$ is only 4% larger from (48), the peak magnitudes for the eigenmodes are some 20% larger (relative to a common asymptotic coefficient as η becomes large), and the momentum flux divergences are similarly magnified. The general function shapes, though, are little different. The quantity B is a small number (0.14), which suggests that the upper layer asymptotics are not badly represented by (35), as an approximation to (36), until quite large values of η.

The parameter dependences of (38) are illustrated in Table 2, which is directly comparable to Table 1. One is again more struck by the similarities rather than the differences between the results of the two approximations. The most important difference, though, occurs when γ approaches K from below [i.e., when $k^2 \ll \Gamma$ in (28), the downstream length scale becomes much greater than the deformation radius]. By the previous assumptions, layer coupling was neglected in the upper layer equation and $\hat{c}$ was consequently independent of γ. A comparison of the second lines in Tables 1 and 2, however, demonstrates that this is inaccurate as $\gamma \to K^-$. A more striking illustration of this $\hat{c}(\gamma)$ dependence arises as K increases. For Eq. (32), there is at least a practical cutoff to solutions around $K = 0.56$,

TABLE 2. Eigenmodes of (38).

(K, γ, δ)	$\hat{c}$	B	$\zeta_{1\max}$	$\xi(\zeta_{1\max})$	$\zeta_{2\max}$	$\xi(\zeta_{2\max})$
(0.5, 0.25, 0.16)	0.48	0.14	0.34	0.33	0.016	0.13
(0.4, 0.25, 0.16)	0.61	0.14	0.42	0.39	0.025	0.11
(0.5, 0.45, 0.16)	0.57	0.13	0.37	0.37	0.052	0.08
(0.5, 0.25, 0.10)	0.47	0.09	0.33	0.32	0.009	0.13

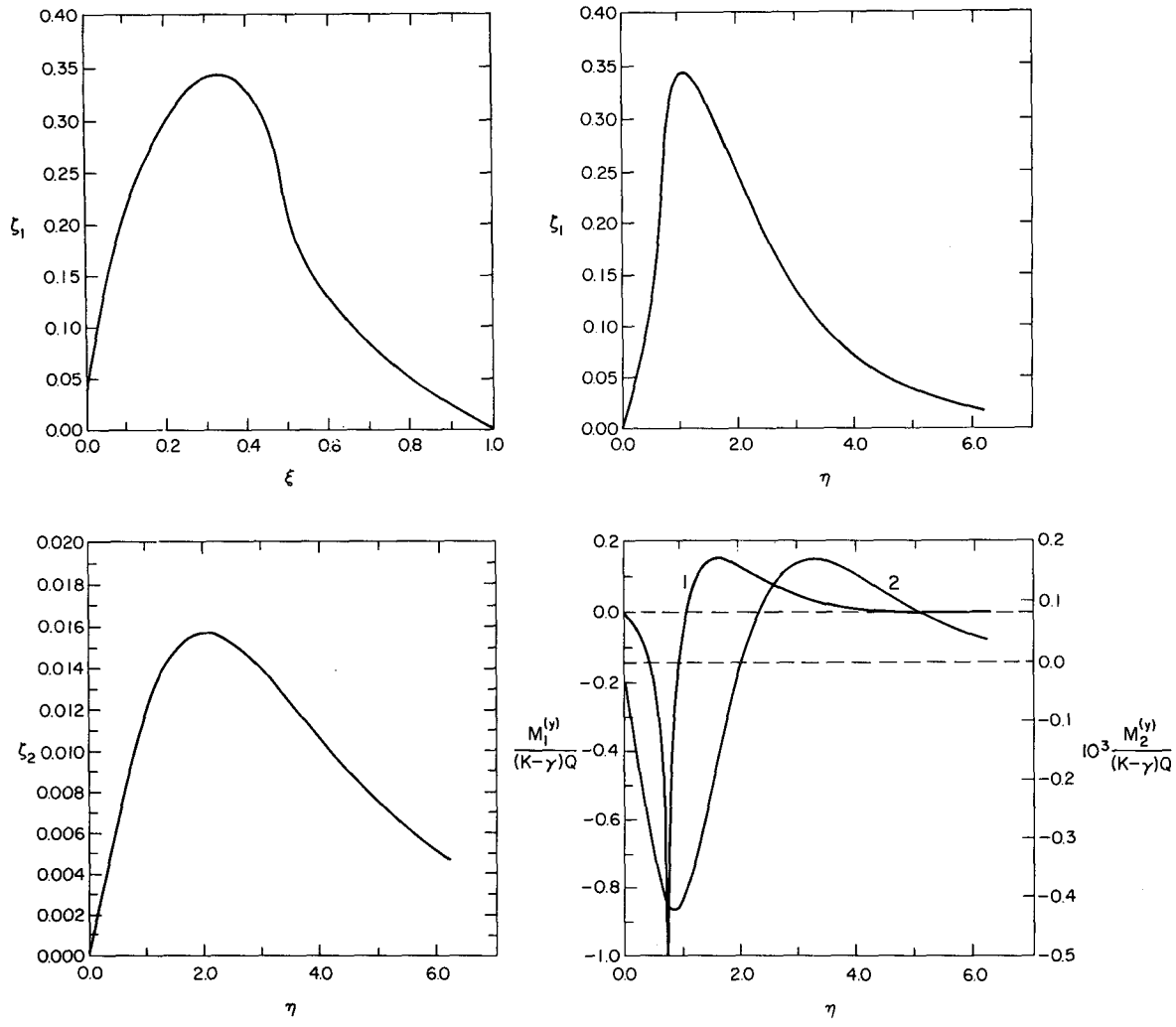

FIG. 2. The counterpart of Fig. 1 from the approximate equations (38). The eigenvalues are $\hat{c} = 0.48$ and $B = 0.14$.

whereas for (38) no such cutoff was found when γ was held fixed at $K - 0.05$ and K increased. In this sequence (shown in Fig. 3), the changes in shape for ζ_1 and ζ_2 are slight, even though their peak amplitudes change considerably. Both $\hat{c}$ and B are decreasing functions of K here. Nevertheless, it remained true for (38), as it was for (32), that there occurred a cutoff to solutions as K was increased for a fixed value of γ.

Many of the parameter dependences of the jet modes may be anticipated from the integrals (29) and (30). In (29), the positive right-hand side should be balanced by both the far-field β term and the layer coupling term. The contribution of the former requires $\hat{c} < \max|\hat{u}_1| = 1$. Furthermore, a larger contribution is needed as K increases; hence $\partial\hat{c}/\partial K < 0$. The contribution of the second term relieves some of the necessity for $\hat{c}$ to decrease to balance an increasing K; hence $\partial\hat{c}/\partial\gamma > 0$. Given the additional fact that the ratio ζ_2/ζ_1 tends to decrease as δ decreases (i.e., upper layer intensification increases as the layer gets thinner), then by a similar argument $\partial\hat{c}/\partial\delta > 0$. From Table 2, we can see that the $\hat{c}(\delta)$ dependence is weak. In the lower layer integral, a balance seems less difficult to explain (i.e., the second term on the right-hand side seems likely to contribute a great deal to the required positive value). Nevertheless, we might expect $\partial\hat{c}/\partial[K + \gamma(\delta - 1)] < 0$ and $\partial\hat{c}/\partial(\partial\gamma) > 0$; both of these tendencies are consistent with the upper layer ones, as well as the Table 2 results.

We now make a dimensional interpretation of these results. If we choose a deformation radius {i.e., $[\Delta g h_0/(1 + \delta)]^{1/2} f_0^{-1}$} of 50 km, $f_0 = 0.7^{-4}\text{s}^{-1}$, $\beta f_0/L = 2^{-1/3}\text{cm}^{-1}\text{s}^{-1}$, $h_0 = 0.75^5$ cm, $L = 2500$ km, and fix the transport by the mean jet (i.e., $V_0 h_0 L\beta/a$) at 30 Sverdrups, then for the standard case of Figs. 1 and 2 we calculate a boundary layer thickness of 30 km and $|\bar{u}'|_{\max} = 140$ cm s^{-1}. The resulting eigenvalue of $\hat{c} = 0.48$ corresponds to a dimensional

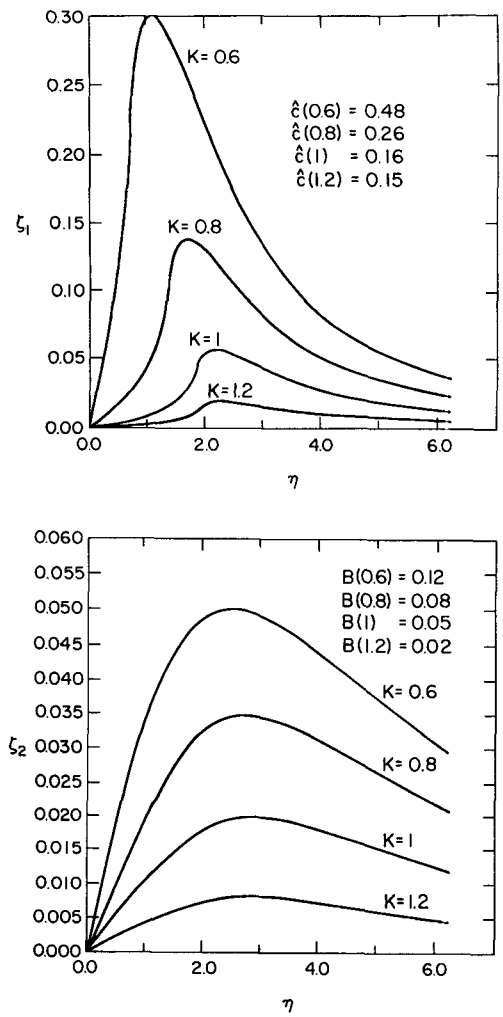

FIG. 3. A sequence of eigenmodes from the equations (38) for $\delta = 0.16$, $\gamma = K - 0.05$ and $K = 0.6$, 0.8, 1.0 and 1.2. The corresponding eigenvalues $\hat{c}(K)$ and $B(K)$ are listed in the upper and lower panels, respectively.

eastward phase propagation at 67 cm s^{-1} for a mode with a wavelength of 350 km. Thus, the parameter range for jet modes is not a wholly unrealistic one compared, say, to the North Atlantic subtropical gyre; the plausibility of the phase speed prediction is discussed in Section 7.

The preceding solutions were obtained using an analytic expansion about the critical layer singularity. Frequently, however, numerical solutions are sought in circumstances where critical layers are present but where tailored local expansions are infeasible (e.g., in the two-dimensional geometry of an enclosed basin rather than a channel—see Section 6). One can always assure the accuracy of standard finite-difference formulas by including sufficient friction, but such a "correction" can transform the dynamical nature of the fluid. Alternatively, the numerical solutions can be accepted with the recognition that they will contain quantitative deficiencies in the neighborhood of critical layers but, one might hope, a qualitatively adequate representation of the grosser features of the true solutions.

This idea can be tested with our present solutions. For Eq. (32) and the parameters of Fig. 1, one can obtain a jet mode solution using the finite-difference formula (A3) through the critical layer [i.e., without matching to the formulas (A6)–(A9)]. The resulting eigenvalue is $\hat{c} = 0.70$ (in contrast to the correct $\hat{c} = 0.46$ which is 30% smaller) and the resulting eigenmode has a qualitatively similar shape to that in Fig. 1 except that $\zeta_{i\max}$ is located closer to the wall. The defect, of course, is due to the inability of a finite-difference representation to resolve the logarithmic singularities which occur in (32) and (A2); this defect is not a strong function of the grid spacing. The parameter tendencies of $\hat{c}$ are indeed qualitatively similar in the purely finite-difference and the correct solutions, but quantitative differences of the order of 50% do occur. Undoubtedly, this discrepancy could lead to false conclusions about some aspects of the solutions.

The solutions we have examined in this section are those of (24), not (13); that is, we have been considering a particularly stringent form of quasi-geostrophy where all of β, $R\Gamma$ and R are vanishing small. For large basins with horizontal dimensions of several thousand kilometers, the first two parameters can be much larger than the last, and many of the eigenmodes can reflect contributions of $O(\beta)$ or $O(R\Gamma)$. For the jet modes, however, we can inquire *a posteriori* whether corrections of these orders could be included in a quasi-geostrophically consistent manner.

The essential quasi-geostrophic approximation is the balance, in the momentum equation, between the horizontal pressure gradient and the Coriolis force. This requires the neglect of the particle accelerations relative to either of these, or $\omega' \ll f'$ (where ω' is a dimensional frequency). This necessary inequality can be alternatively expressed in terms of the nondimensional quantities of our jet mode solutions,

$$\beta\hat{c}\left\{\begin{matrix}\hat{K}\\ \text{or}\\ \dfrac{\partial}{\partial\eta}\end{matrix}\right\} \ll 1 + \beta\Delta y,$$

where $\hat{K} = (K^2 - \gamma)^{1/2}$. Thus, for jet modes with order unity values for $\hat{c}$, $\hat{K}$ and ∂_η, the inequality is satisfied for $\beta \ll 1$, but it is not so strongly satisfied that the second term on the right-hand side can be consistently retained relative to the neglected ageo-

strophic particle accelerations. Thus, for jet modes, the differences between Eqs. (24) and (13) are unimportant. As a general proposition, it will only be modes with small phase speed and/or large horizontal scale that the less restrictive approximations of (13) will be meaningful.

5. A double-gyre solution

In Sections 3 and 4, various quantities were derived for a mean zonal jet on the northern wall of a zonal channel. With only slight alterations, we can also consider the case of a narrow, eastward jet in the center of the channel with weak, westward return flows on either side. This solution for the mean flow is a special case of Eqs. (11) and (12), where the constants a, b and c are, in principle, different in the northern and southern halves of the basin. Their particular values are chosen so that, in a basin extending from 0 to 2 in y, there are no boundary layer jets on $y = 0$ and 2, and both $\bar{\psi}_1(y)$ and $\bar{h}_1(y)$ are continuous and have continuous first derivatives at $y = 1$. The choices which permit this are

$$\begin{aligned} a^N &= a^S \\ \begin{cases} b^N = 1 + \beta \\ b^S = 1 - \beta \end{cases} \\ c^N &= c^S \end{aligned} \tag{39}$$

(in an expansion in R), where now the Coriolis parameter has been centered at the jet [i.e., $y_0 = 1$ in (4)] and the superscripts N and S refer to $y > 1$ or $y < 1$, respectively. The resulting solution is identical to (23) with odd symmetry in ψ about $y = 1$. The resulting mean zonal velocity profile

$$\bar{u}_1(y) = -\partial\bar{\psi}_1/\partial y = -\beta/a + (\beta/a)Q/\sinh Q \times \begin{cases} \cosh Qy, & y < 1 \\ \cosh Q(2 - y), & y > 1 \end{cases} \tag{40}$$

has a cusp at $y = 1$. While no doubt the addition of a small amount of friction to the mean equations (7) would smooth out this cusp, we shall not do this here in order to retain the guarantee of stability from (10) [n.b., $\partial\bar{P}_1/\partial\bar{\psi}_1 = a > 0$ over the whole domain of the double gyre (40)]. In reality, cusps cannot exist, but neither would a strong mean jet likely be absolutely stable in the ocean.

Because the mean profile (23) remains valid for the southern half of the double gyre and the northern half is identical by a negative reflection, then the eigenvalue differential equations (24)–(25) apply for the double gyre as well if we wish to solve for either the symmetric or anti-symmetric eigenmodes. For the latter modes, $\zeta_1 = \zeta_2 = 0$ at $y = 1$, and the solutions of Sections 3 and 4 are appropriate here as well. For the former modes, the only alteration to Section 3 is in the $y = 1$ boundary conditions; for symmetric double gyre modes, we require

$$\partial\zeta_1/\partial y = \partial\zeta_2/\partial y = 0 \quad \text{at} \quad y = 1.^5 \tag{41}$$

These conditions require that the shooting targets in (A2) and (A12) be changed to (A19) and (A20); otherwise the formulas of the Appendix are applicable for this case as well.

Shown in Fig. 4 is a double-gyre symmetric solution for the same parameters as in Figs. 1 and 2. This particular solution is from the Eqs. (38) and (41). If the more approximate equations (34) had been used, then a similar level of discrepancy would occur as in the single gyre modes described in Section 3; for this section, only the more accurate eigenmodes will be presented.

In Fig. 4, the eigenmodes have their maximum amplitudes at the center of the jet ($\eta = 0$) instead of on the wings; the lower layer amplitudes are not as weak relative to the upper ones; there is no critical layer (i.e., $\hat{c} > 1$); the asymptotic layer coupling is stronger (i.e., B has increased from 0.14 to 0.22); and the momentum flux divergences are stronger and of one sign in $y < 1$ (n.b., they will be antisymmetric about $y = 1$, implying a forcing of a mean meridional divergence about the center of the jet).

The absence of a critical layer can be justified heuristically from the upper layer integral (29). For the symmetric mode conditions (41), the final term does not vanish as before; rather it contributes

$$\frac{\zeta_1^2(1)}{\hat{c} - 1}\frac{\beta}{R}\tanh Q. \tag{42}$$

This is a large positive number for $\hat{c} > 1$, and it can serve as the primary balance for the left-hand side terms in (29), supplanting the first right-hand side term from which was previously obtained the $\hat{c} < 1$ condition. This result is somewhat artificial since it depends upon the existence of the cusp in the mean velocity (i.e., $\hat{u}_\eta \neq 0$ at $\eta = 0$).

The parametric dependences for the symmetric, double-gyre modes are shown in Table 3. In general the tendencies are the same as for the single-gyre case; we note that $\partial\hat{c}/\partial K < 0$, $\partial\hat{c}/\partial\gamma > 0$, $\partial B/\partial\delta > 0$, and, weakly, $\partial\hat{c}/\partial\delta > 0$ and $\partial B/\partial K < 0$. The exception is that now $\partial B/\partial\gamma$ is a large positive number rather than the weak positive number indicated in Table 2. There are no difficulties in obtaining solutions for the double-gyre modes, neither as K gets very small or very large. This latter is contrary to the single-gyre case, no doubt because

[5] Ambiguity between the claimed symmetries and the $y = 1$ boundary conditions could arise if there existed modes with simultaneously $\zeta_i = \partial\zeta_i/\partial y = 0$ at $y = 1$. None were found, although no special search was made for them.

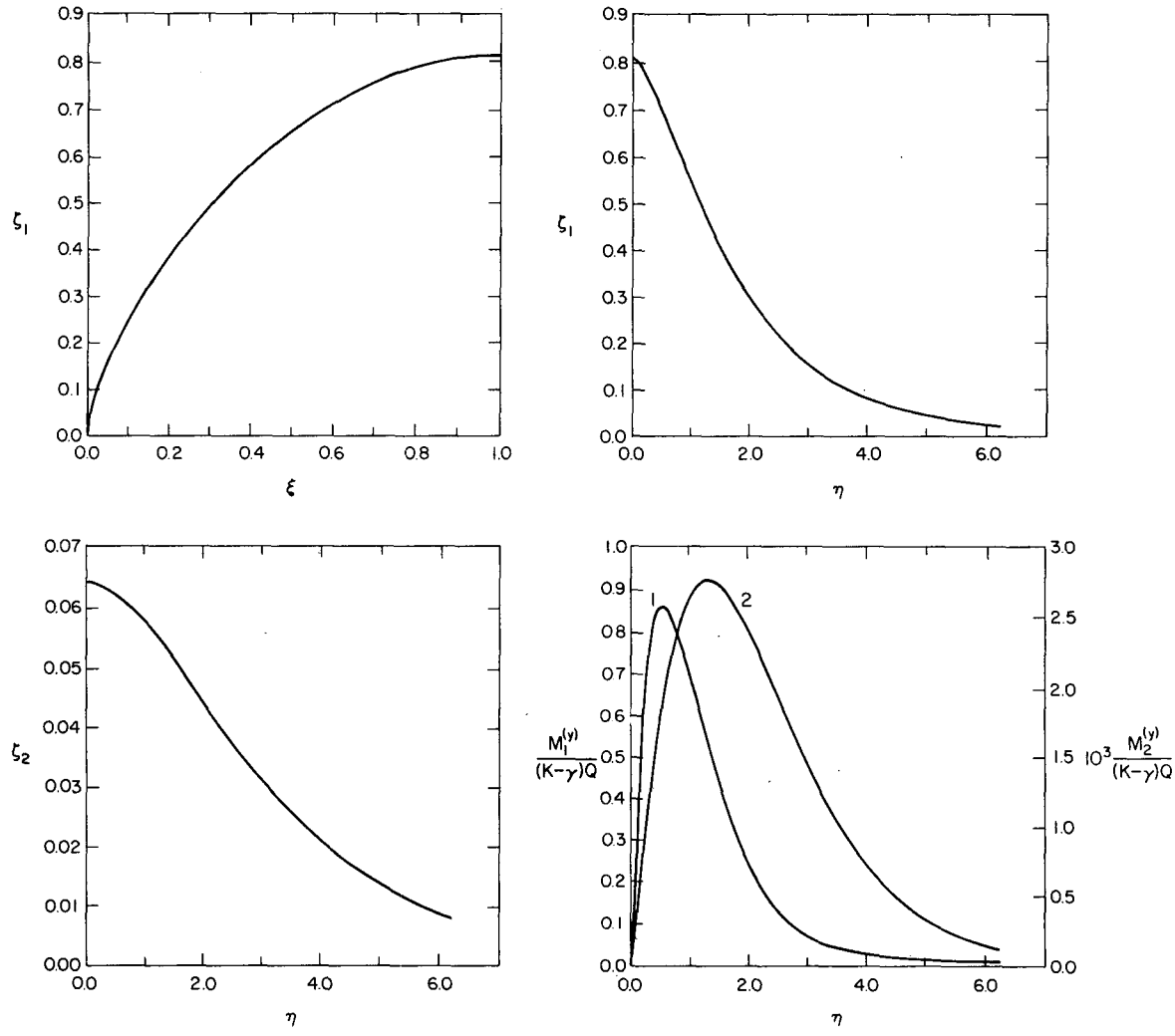

FIG. 4. A symmetric, double-gyre jet mode from Eqs. (38) and (41). The parameters selected were $K = 0.5$, $\gamma = 0.25$ and $\delta = 0.16$. The eigenvalues are $\hat{c} = 1.46$ and $B = 0.22$.

the differential equation singularities no longer can coalesce by $\hat{c}$ decreasing toward zero. A dimensional interpretation for the Fig. 4 solution, analogous to that given at the end of Section 4, is that the mean jet transports 60 Sverdrups to the east within a width of 60 km, (i.e., $\Delta\eta = 2$), and the resulting jet mode has a phase speed to the east at 200 cm s^{-1}.

6. Basin modes

In this section several eigenmodes to the two-dimensional equation (13) are presented for a square

TABLE 3. Eigenmodes of (38) with (41).

(K, γ, δ)	$\hat{c}$	B	$\zeta_1(1)$	$\zeta_2(1)$	$\left\lvert \frac{M_1^{(\nu)}}{Q(K-\gamma)}(\xi) \right\rvert_{\max}$	$\left\lvert 10^3 \frac{M_2^{(\nu)}}{Q(K-\gamma)}(\xi) \right\rvert_{\max}$
(0.5, 0.25, 0.16)	1.46	0.22	0.82	0.064	0.86 (0.58)	2.8 (0.26)
(0.4, 0.25, 0.16)	1.60	0.26	0.85	0.099	0.84 (0.56)	5.6 (0.21)
(0.5, 0.45, 0.16)	1.71	0.51	1.07	0.35	1.08 (0.52)	54.0 (0.16)
(0.5, 0.25, 0.10)	1.45	0.14	0.76	0.038	0.75 (0.58)	1.0 (0.26)
(0.2, 0.1, 0.16)	2.07	0.225	0.88	0.064	0.69 (0.45)	1.9 (0.13)
(1, 0.25, 0.16)	1.21	0.18	0.78	0.024	1.12 (0.69)	0.6 (0.41)
(1, 0.95, 0.16)	1.53	0.77	1.21	0.60	1.6 (0.57)	200.0 (0.24)

ocean basin. The simplifications resorted to in Sections 3–5 are, for the most part, abandoned; only the rigid lid approximation [$\Delta = 0$ in (11), (14), (18) and (22)] is retained. On the other hand, the numerical techniques which were used to obtain these basin modes (see the Appendix) have two major defects, both of which likely introduced significant quantitative errors. The first of these defects is the lack of a correct critical layer representation [as, for example, in (A6)]. As discussed for the channel case in Section 4, this defect can lead to errors in the phase speed and the location of eddy extrema on the order of 50%. The second defect is a marginally inadequate spatial resolution for many of the eigenmodes. For the maximum, economically feasible numerical resolution (described in the Appendix), some features of the modes—particularly the phase speeds of the jet modes—are not yet invariant with respect to resolution (the remaining resolution errors are of the order of 20% in c). Nevertheless, jet modes were present in each of a large number of examples considered by the investigator. Thus, it seems highly probable that basin modes of the general character of those shown below always do exist and that these examples fairly demonstrate the occurrence, under more general circumstances, of the jet modes more rigorously derived in the channel geometry with $\{R,\beta,R\Gamma,Q^{-1}\} \to 0$.

Solutions to (12)–(13) will be shown for only a single set of parameter values; *viz.*,

$$R = 1.4 \times 10^{-4} \qquad a = 0.025$$
$$\delta = 0.11 \qquad b = 0.86$$
$$\beta = 0.27 \qquad c = -11$$
$$\Gamma = 100 \qquad Q = 13$$
$$\sigma = 0$$

These are not accurate values for the North Atlantic Ocean. In order to minimize the resolution defect, the parameters (43) have been chosen to represent a basin which is either too small or has too broad a boundary current width ($\sim Q^{-1}$) and which is excessively stratified so that the deformation radius ($\sim \Gamma^{-1/2}$) is too large. Fig. 5 shows the nondimensional solutions for $\bar{\psi}_1$ and $\bar{h}_1$. They exhibit a broad interior region of nearly uniform westward flow, with stronger and narrower return flows near the walls. There is also a weak westward current adjacent to the southern wall, even though (43) implies $b = 1 - \beta/2$, which is sufficient to eliminate the southern wall current in the asymptotic limits of Section 3. $\bar{\psi}_1$ and $\bar{h}_1$ do not have the numerical defects discussed above.

A first example of the basin modes for Fig. 5 is shown in Fig. 6. This is not a jet mode but a slightly altered gravest barotropic mode. Asymptotically as $\{\beta,R\} \to 0$ in a quiescent ocean ($\bar{\psi}_1 = 0$, $\bar{h}_1 = 1$), this mode would have the form

$$\zeta_1 = \zeta_2 = \sin\pi y \sin\pi x[\cos(\beta/2\omega R)(x - \tfrac{1}{2}) - i \sin(\beta/2\omega R)(x - \tfrac{1}{2})], \quad (44)$$

where

$$\omega = \beta/(2\sqrt{2}\,\pi R). \quad (45)$$

This quiescent solution is closely related to the channel solution (26), and, furthermore, is similar to the basin mode in Fig. 6. The major differences in the basin mode are a 7% reduction of the frequency [n.b., $\omega = 217$ is predicted from (43) and (45)] and the appearance of some smaller scale structure in ζ_1 in the basin interior; ζ_2 is remarkably similar to (44). The momentum flux divergences M_i, from (20), are also shown in Fig. 6. The M_2 patterns have a large spatial scale and correspond to what would result from the quiescent modes (44). In the upper layer, however, the small amplitude departures from (44) dominate M_1; the patterns are of relatively small scale and would tend to force a secondary mean

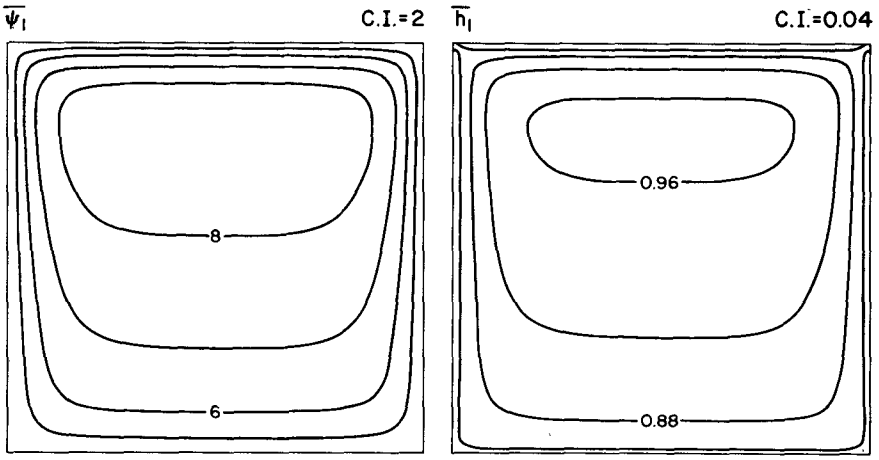

FIG. 5. The mean streamfunction ψ_1 and layer thickness h_1 for the upper layer. These are solutions of (11)–(12) for the parameters (43). "C.I." is an abbreviation for contour interval.

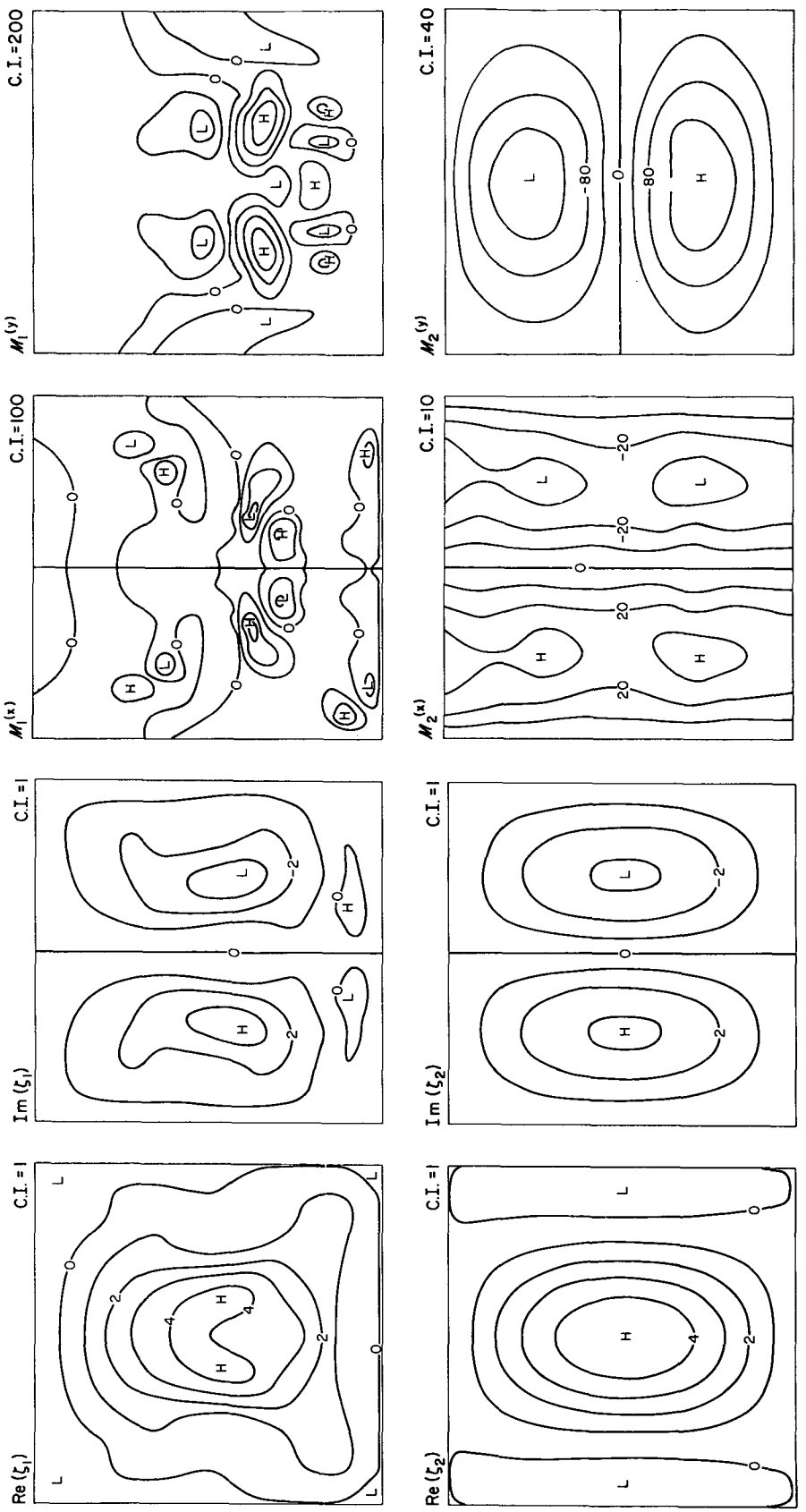

FIG. 6. A basin mode from (13) and (43), which is qualitatively similar to the gravest barotropic mode (44)–(45). The pressure patterns correspond to times separated by a quarter period [with $\mathrm{Re}(\zeta_j)$ leading $\mathrm{Im}(\zeta_j)$]. The frequency is $\omega = 202$. The M_j are calculated for a mode normalization such that

$$\max_{(x,y)} |\mathrm{Re}(\zeta_j)| = 1.$$

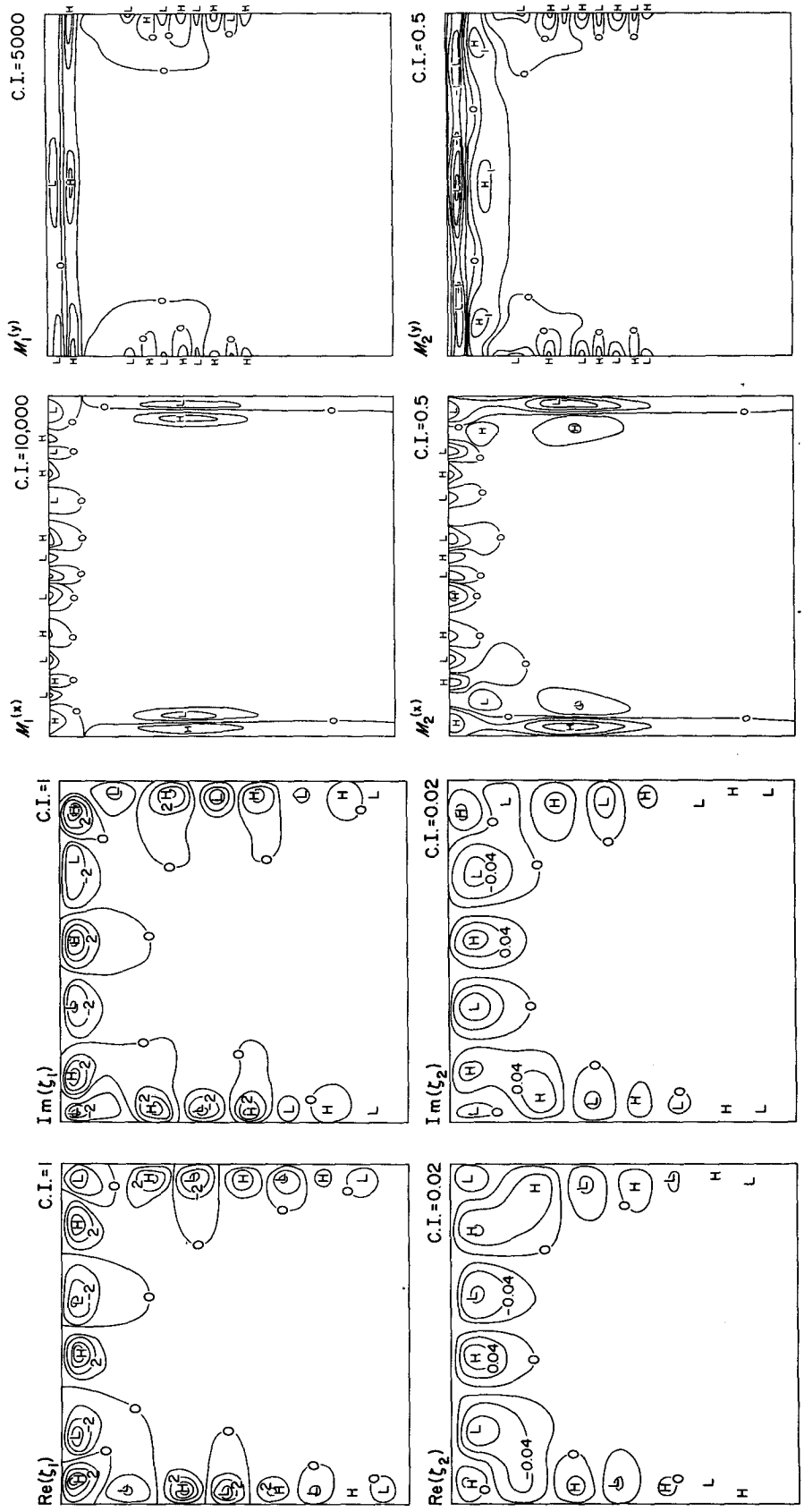

FIG. 7. A basin mode presented in the same format as Fig. 6. Here the mode is of the jet mode type. $\omega = 1990$.

circulation primarily away from the boundary jets. In general, the basin modes contain many examples of slightly altered quiescent barotropic modes; as their spatial scale decreases the alterations due to the mean gyre increase. No examples were found of slightly altered quiescent baroclinic modes; since in a closed basin they necessarily have a small zonal scale of $O(\Gamma^{-1/2})$—unlike the channel baroclinic modes (26)—it is perhaps not surprising that the mean gyre influences are strong.

Finally, an example of a closed basin mode which is approximately a jet mode is shown in Fig. 7. We can recognize the structural features identified in the channel solutions of Section 4: this basin mode is confined to the region of strong mean currents, its eddies are vertically in phase but strongest in the upper layer, its horizontal scale is broadest in the lower layer, and its phase propagation is in the direction of the mean jet.

An identification of the jet mode wavelength can only be done approximately since it varies from eddy to eddy. However, if we identify π/k with the typical separation of eddy centers along the northern wall, then we can calculate the jet mode parameters defined in (28). They are $\gamma = 0.6$, $K = 2$ and $\hat{c} = 0.8$, which at least qualitatively match those of the previous, more exact solutions.[6] $\hat{c} \lesssim 1$ is again the statement that the jet mode has a phase speed somewhat less than the maximum speed of the mean jet.

The patterns of momentum flux divergence for this jet mode are also shown in Fig. 7. These patterns are again such as to force a divergence in both layers along the axis of the mean jet. In addition, there are some eddy-scale structures which would locally accelerate or decelerate the jet in the direction of its flow. This latter tendency is absent in the channel jet modes; it also has a scale comparable to the resolution scale for the mode calculation and is therefore numerically questionable. The heat flux divergence $\mathcal{H}$ is nonzero for the mode in Fig. 7—again in contrast to the channel jet mode—but its amplitude is small compared to what one would estimate from a scale analysis of the ζ_1 and ζ_2 patterns.

In addition to the mode in Fig. 7, there exist many other basin modes for the mean gyre in Fig. 5 which have the general character of jet modes. They differ from each other in their wavelength along the jet and the extent to which they extend along the perimeter of the basin and, consequently, in their phase speed and ζ_1/ζ_2 ratio.

[6] The match is particularly good with the channel solutions obtained without a local critical layer expansion. Recall that they did not exhibit an upper limit on the value of $K - \gamma$ for which solutions could be obtained (Section 4).

7. The jet mode as an archetype

The solutions which have been presented in Sections 3–6 are valid for very particular geometries and mean flow profiles. I offer the conjecture, however, that the qualitative features of these jet modes will be reproduced under much more general circumstances. When the mean jets are strong [i.e., their local Rossby numbers are much larger than the non-dimensional β from (5)] and narrow [their widths are not larger than the deformation radius], there should be eigenmodes whose amplitudes are small away from the jet and whose phase speed is in the direction of the jet. Furthermore, when the jet is layer intensified as here, the jet modes are as well, and the lower layer, cross-jet scale is larger than the upper. The parameter dependences of the phase speed should perhaps also be as described in Sections 4 and 5. This conjecture will not be proved here; its final demonstration rests on finding enough theoretical results and at least a few observations which conform to it.

Let us consider those statements which can be made fairly generally. If there exists a mean profile $\bar{u}(y)$ and parameters and scales which correspond to the assumptions preceding Eq. (24), then that equation is generally valid if we write the potential vorticity gradients without recourse to (11). In general, for small β, R and $R\Gamma$,

$$\mathcal{P}_1 = 1/Q - \hat{u}_{1\eta\eta}, \quad \mathcal{P}_2 = 1/Q - \delta\gamma\hat{u}_1. \qquad (46)$$

If the mean velocity vanishes away from a "jet region", then from (46) we recover (36) for the eigenmodes. That relation implies exponential decay for the modes away from the jet, thus assuring their effective "trapping" within the jet region. The relative weakness of the lower layer eigenmode is also assured by (42), in the layer-decoupled approximation (33), because of the smallness of the parameter $\delta\gamma$. This quantity is small both for oceans with shallow thermoclines (where $\delta \ll 1$) and where $R\Gamma \ll 1$, as has been previously assumed. Note that $\gamma = R\Gamma/a$ from (23) and (28); thus, the solutions of Sections 4 and 5 are formally only valid for small γ.

The parameter dependences of the eigenvalue $\hat{c}$ on K, γ and δ have all been heuristically identified from the integral constraints (29) and (30); for more general "strong and narrow" $\hat{u}_1(\eta)$ jet profiles, many of the same tendencies should persist. These integrals are real ones only for stable eigenmodes. For the case of complex $\zeta_i(\eta)$ and $\hat{c}$, one can derive a pair of such integrals [as in Pedlosky (1964)]; in such a case, however, it is more difficult to identify the parameter dependences of $\mathrm{Re}\{\hat{c}\}$, except when $\mathrm{Im}\{\hat{c}\}$ is relatively small (i.e., the instability is weak). Nevertheless, it is often true that actual solutions for unstable modes share many of the characteristics of the jet modes presented here. In the case of a

"Bickley Jet" [$\bar{u}(y) = \text{sech}^2 y$], for example, the real part of the phase speed was found to be a decreasing function of the zonal wavenumber for modes of odd symmetry and an increasing function for even modes (Drazin and Howard, 1966). The former property matches the result of Section 4, while the latter conflicts with that of Section 5; again it seems as if a cusp in the mean jet profile yields peculiar modal behavior.

In Haidvogel and Holland (1978), a parameter study of the most unstable modes was made for a particular class of narrow jets (ones without any special potential vorticity properties, however). The maximally unstable modes they examined did exhibit strong trapping in the upper layer and within the jet region; the pressures were more often than not nearly in phase in the two layers; the lower layer patterns showed a horizontal scale expansion relative to the upper; and the parameter dependences $\delta\hat{c}/\partial\delta > 0$ (except for some anomalous behavior for very small δ) and $\partial\hat{c}/\partial\gamma \gtrsim 0$ for small γ were found ($\partial\hat{c}/\partial K$ was not tested). One discrepancy was that their maximum jet velocity exceeded the eastward phase speed (unlike Section 5), but, of course, their mean velocity had no cusp. In a similar manner the spatial structure of the unstable modes found by Orlanski and Cox (1973) qualitatively matched the jet mode structures (n.b., their Figs. 3–4).

Another situation where transient eddies have exhibited jet mode characteristics is reported in McWilliams *et al.* (1977). From a numerical simulation of the statistical equilibrium state of a steadily forced, two-layer channel flow, calculations were made of the principal components of streamfunction variance (i.e., the eigenmodes of the matrix $\overline{\psi(\mathbf{x}_i,t)\psi(\mathbf{x}_j,t)}(dV_i dV_j)^{1/2}$, where ψ is the streamfunction, the overbar is a time average and dV_i the fractional volume element associated with the gridpoint $\mathbf{x}_i$). These principal components were found to usually occur in pairs, approximately displaced from each other by a quarter-cycle in time and the zonal direction, and thus representing zonal propagation. Their phase speed was in the direction of the mean jet, they vanished outside the jet, and they were vertically in phase and upper-layer intensified (though less so than the solutions of Sections 4–6 because there was a mean lower layer jet as well). The pairs which were evenly symmetric about the jet center had an increasing phase speed with increasing zonal wavenumber, which is a further indication that the $\partial\hat{c}/\partial K < 0$ tendency found in Section 5 is not generally characteristic of the symmetric modes of thin jets away from boundary walls. Some of the principal component pairs were baroclinically unstable (i.e., they provided a significant rate of conversion of mean potential to eddy potential energy) and some were not.

The jet modes provide at least one potentially very important observational caution. In the North Atlantic subtropical gyre, the low-frequency variance is largest in the vicinity of the Gulf Stream (Schmitz, 1976). It has been argued that this is evidence for this region as a generating one for fluctuations by an instability (or else why should the amplitudes be largest there?). However, the stable modes presented here also have their amplitude maxima in the jets, and the conclusion of local eddy generation is not a necessary one. There are at least some aspects of the observations, though, which are not well explained by jet modes; for example, Hansen's (1970) eastward phase speeds for Gulf Stream meanders are an order of magnitude smaller than the dimensional values discussed above, though it is doubtful whether his observational techniques would have detected rapid phase speeds. Robinson *et al.* (1974) do refer to "large-scale variations" in the Gulf Stream with a length scale of 40 km and a time scale of approximately a day. While these scales approximately match jet mode scales, their observational documentation is as yet very crude. Luyten (1977) did not observe rapid zonal propagation from a bottom array of current meters beneath the Gulf Stream but little jet mode signal would be expected at this depth.

In summary, the theoretical evidence generally supports the usefulness of jet modes as an archetype for ocean transience, while the observational evidence is inconclusive. The structural form of the solutions presented here may be their most generalizable characteristic, while their stability and predicted dispersion relation may be valid only in much more restricted circumstances.

Acknowledgments. This research was supported by the National Science Foundation through its grant to the National Center for Atmospheric Research. Computational assistance was provided by J. H. S. Chow, and the manuscript was prepared by Karla Nolan. I am particularly grateful to J. E. Hirsh who shared his finite element algorithms for the computations of Section 7. This paper is MODE Contribution No. 91.

APPENDIX

Numerical Solution Techniques

To solve the upper-eigenvalue equation of Eqs. (34), we convert the system to one of first order in y and explicitly extract the leading order asymptotic term as $\zeta \to 0$; that is, we define

$$Z = \xi^{-K^{1/2}}\zeta_1,$$

$$Y = (\hat{c} - \xi)\xi^{-K^{1/2}}[\xi_1' - (K^{1/2}/\xi)\zeta_1], \quad \text{(A1)}$$

and write the eigenvalue problem as

$$\left.\begin{aligned} Z' &= Y/(\hat{c} - \xi) \\ \xi Y' &= -Z - [2\sqrt{K} + 1 + \xi/(\hat{c} - \xi)]Y \\ Z(0) &= 1, \quad Y(0) = -(2\sqrt{K} + 1)^{-1} \\ Z(1) &= 0 \end{aligned}\right\}. \quad \text{(A2)}$$

This coupled system will be solved by initially guessing a value for $\hat{c}$ and then integrating away from $\xi = 0$ by Runga-Kutta finite-difference formulas. For example, for the first equation in (A2) we write

$$Z_{i+1} = Z_i + \tfrac{1}{2}\Delta\xi Y_i\left[\frac{1}{\hat{c} - \xi_i} + \frac{1}{\hat{c} - \xi_{i+1}} \times \left(1 + \Delta\xi \frac{1}{\hat{c} - \xi_i}\right)\right] \quad \text{(A3)}$$

to obtain a value of $Z_{i+1} \equiv Z(\xi_{i+1})$ from dependent variables at lower values of $\xi_j = \Delta\xi(j - 1)$. The integration proceeds until $\xi_{N+1} = 1$, where Z_{N+1} is tested for a zero value. If it is nonzero, a new $\hat{c}$ guess is made and the integration is repeated. This iteration process is continued until Z_{N+1} converges to zero.

The formula (A3) is inadequate near a singular point of (A2). The first singular point is at $\xi = 0$. There a simple Taylor series expansion is of the form

$$\left.\begin{aligned} Z_0(\xi) &= 1 + \sum_{j=2}^{M_0} \frac{1}{(j-1)!} A_j \xi^{j-1} \\ Y_0(\xi) &= -\frac{1}{(2\sqrt{K} + 1)} + \sum_{j=2}^{M_0} \frac{1}{(j-1)!} B_j \xi^{j-1} \end{aligned}\right\}, \quad \text{(A4)}$$

where $A_2 = -1/[\hat{c}(2\sqrt{K} + 1)]$ and

$$\left.\begin{aligned} (2\sqrt{K} + j)B_j &= -jA_j \\ \hat{c}A_{j+1} &= (j - 1)A_j + B_j \end{aligned}\right\} \quad \text{(A5)}$$

for $j > 2$. This expansion is used to evaluated Z and Y from $\xi = 0$ to an intermediate ξ_0 (in practice $0.05 \leq \xi_0 \leq 0.1$) where $Z_0(\xi_0)$ and $Y_0(\xi_0)$ are used as starting values for the Runga-Kutta integration (A3). The solutions obtained were not overly sensitive to the values used for ξ_0 and M_0.

The other singular point for (A2) occurs at the critical layer $\xi = \hat{c}$, assuming $\hat{c}$ is real and between 0 and 1—the first is assured by the stability of the mean flow (Section 1) and the second always occurs for the particular profile (23). Here again an explicit expansion is employed. We define a critical layer independent variable $\tau = \xi - \hat{c}$. The Runga-Kutta integration proceeds up to $-\tau_0$ from below and from τ_0 to more positive values of τ; in between the solutions are evaluated by the expansion, whose free constants are chosen by matching to the Runga-Kutta values at $-\tau_0$ and which provides starting values at $+\tau_0$ for (A3). There are two linearly independent solutions to (A2) near $\tau = 0$, and the matching at $-\tau_0$ provides their constant coefficients for a given $\hat{c}$ value. These two solutions are

$$\left.\begin{aligned} Z_1(\tau) &= 1 + \sum_{m=1}^{M_1} (a_m + b_m \ln|\tau/\hat{c}|)\tau^m \\ Y_1(\tau) &= -\sum_{m=1}^{M_1} (ma_m + b_m + mb_m \ln|\tau/\hat{c}|)\tau^m \end{aligned}\right\}, \quad \text{(A6)}$$

where $a_1 = 0$, $b_1 = 1/\hat{c}$, and

$$\left.\begin{aligned} b_m &= -(-\hat{c})^{-m} \prod_{j=2}^{m}\left[1 - \frac{1}{j-1} + \frac{2\sqrt{K}}{j}\right] \\ a_m &= -\frac{(2m-1)}{m(m-1)} b_m \\ &\quad - \frac{1}{\hat{c}}\left[1 - \frac{1}{m-1} + \frac{2\sqrt{K}}{m}\right] a_{m-1} \\ &\quad - \frac{2}{\hat{c}}\left[\frac{\sqrt{K} + m - 1}{m(m-1)}\right] b_{m-1} \end{aligned}\right\} \quad \text{(A7)}$$

for $m = 2, \ldots, M_1$, and

$$\left.\begin{aligned} Z_2(\tau) &= -\tau - \sum_{m=1}^{M_2} c_m \tau^{m+1} \\ Y_2(\tau) &= \tau + \sum_{m=1}^{M_2} (m + 1)c_m \tau^{m+1} \end{aligned}\right\}, \quad \text{(A8)}$$

where

$$c_m = \prod_{j=1}^{m}\left(-\frac{j(2\sqrt{K} + j) - 1}{\hat{c}j(j+1)}\right), \quad \text{(A9)}$$

for $m = 1, \ldots, M_2$. Again the results were not overly sensitive to the values chosen for τ_0, M_1 and M_2.

The lower equation in (34) was solved as a matrix problem for the vector $\zeta_2(\xi_i)$, $i = 1, \ldots, N$, with a second-order difference approximation to the differential equation and $\zeta_1(\xi_i)$ obtained by the procedure described above. The singularity at $\xi = 0$ gave no difficulty, and there is no singularity at the critical layer through two derivatives of $\zeta_2(\xi)$.

To solve the layer coupled eigenvalue equation (38), we redefine the independent variable as $\xi = e^{-\eta}$ and define additional dependent variables,

$$y_1(\xi) = (\hat{c} - \xi)\zeta_1'(\xi), \quad y_2(\xi) = \xi\zeta_2'(\xi). \quad \text{(A10)}$$

In terms of these quantities, the system of first-order equations to be solved is (A10) plus

$$\left.\begin{aligned} y_1' &= -[1/\xi + 1/(\hat{c} - \xi)]y_1 \\ &\quad - \left(1/\xi - K\frac{\hat{c} - \xi}{\xi^2}\right)\zeta_1 - \gamma\frac{\hat{c} - \xi}{\xi^2}\zeta_2 \\ y_2' &= \left[\frac{K - \gamma(1 - \delta)}{\xi} - \frac{\delta\gamma}{\hat{c}}\right]\zeta_2 - \frac{\delta\gamma}{\xi}\zeta_1 \end{aligned}\right\}. \quad \text{(A11)}$$

The Runga-Kutta integration procedure will again be as illustrated in (A3); now, however, the iteration will be in $\hat{c}$ and B values, until

$$\zeta_1(\xi_{N+1}) = \zeta_2(\xi_{N+1}) = 0. \tag{A12}$$

The system (A10)–(A11) again has two singular points, at $\xi = 0$ and $\hat{c}$. Near $\xi = 0$, we represent the solution as

$$\left.\begin{aligned} \zeta_1 &= \zeta_{11} + B\zeta_{12}; \quad y_1 = y_{11} + By_{12} \\ \zeta_2 &= \zeta_{21} + B\zeta_{22}; \quad y_2 = y_{21} + By_{22} \end{aligned}\right\}. \tag{A13}$$

The individual terms in (A13) are

$$\left.\begin{aligned} \zeta_{1j} &= \sum_{n=0}^{N_0} \alpha_{jn}\zeta^{n+e_j} \\ y_{1j} &= \alpha_{j0}e_j\hat{c}\xi^{e_j-1} \sum_{n=0}^{N_0} [\hat{c}(n + 1 + e_j)\alpha_{j,n+1} \\ &\qquad - (n + e_j)\alpha_{jn}]\xi^{n+e_j} \\ \zeta_{2j} &= \sum_{n=0}^{N_0} \beta_{jn}\xi^{n+e_j} \\ y_{2j} &= \sum_{n=0}^{N_0} (e_j + n)\beta_{jn}\xi^{n+e_j} \end{aligned}\right\} \tag{A14}$$

for $j = 1, 2$ and

$$\left.\begin{aligned} &\alpha_{j,n+1}[\hat{c}(n + 1 + e_j)^2 - \hat{c}K] + \beta_{j,n+1}\hat{c}\gamma \\ &\qquad = \alpha_{jn}[(e_j + n)^2 - 1 - K] + \beta_{jn}\gamma \\ &\beta_{j,n+1}[(e_j + n + 1)^2 - K + \gamma(1 - \delta)] \\ &\qquad + \alpha_{j,n+1}\delta\gamma = -\delta\gamma/\hat{c}\beta_{j,n+1} \end{aligned}\right\} \tag{A15}$$

for $n = 0, \ldots, N_0 - 1$, where

$$\left.\begin{aligned} e_1 &= (K + \delta\gamma)^{1/2}, \quad \alpha_{10} = 1, \quad \beta_{10} = -\delta \\ e_2 &= (K - \Gamma)^{1/2}, \quad \alpha_{20} = 1, \quad \beta_{20} = 1 \end{aligned}\right\}. \tag{A16}$$

The critical layer expansion [the counterpart of (A6) and (A8)] now consists of a sum of four independent solutions, each of which can be written in the form

$$\left.\begin{aligned} \zeta_{ij}(\tau) &= \sum_{n=1}^{N_1} (a_{jm} + \ln|\tau/\hat{c}|\, b_{jn})\tau^n + a_{j0} \\ y_{ij}(\tau) &= -\sum_{n=1}^{N_1} (na_{jn} + b_{jn}[1 + n \ln|\tau/\hat{c}|]\tau^n \\ \zeta_{2j}(\tau) &= c_{j0} + \sum_{n=1}^{N_1} (c_{jn} + \ln|\tau/\hat{c}|\, d_{jn})\tau^n \\ y_{2j}(\tau) &= \hat{c}(c_{j1} + d_{j1}) + \hat{c}d_{j1} \ln|\tau/\hat{c}| \\ &\quad + \sum_{n=1}^{N_1} \{nc_{jn} + d_{jn} + \hat{c}(n + 1)c_{j,n+1} \\ &\qquad + \hat{c}d_{j,n+1} + \ln|\tau/\hat{c}|[nd_{j,n} \\ &\qquad + (n + 1)\hat{c}d_{j,n+1}]\}\tau^n \end{aligned}\right\}, \tag{A17}$$

for $j = 1, 2, 3, 4$, with recursion relations (deleting the j subscripts)

$$\left.\begin{aligned} &a_{n+1}[n(n + 1)] + b_{n+1}[2n + 1] \\ &\quad = a_n[(n + 1 - 2n^2)/\hat{c}] + b_n(1 - 4n)/\hat{c} \\ &\qquad + a_{n-1}[1 + K - (n - 1)^2]/\hat{c}^2 \\ &\qquad\quad + b_{n-1}[2(1 - n)/\hat{c}] - c_{n-1}\gamma/\hat{c}^2 \\ &b_{n+1}[n(n + 1)] = b_n[(n + 1 - 2n^2)/\hat{c}] \\ &\qquad + b_{n-1}[1 + K - (n - 1)^2]/\hat{c}^2 - d_{n-1}\gamma/\hat{c} \\ &c_{n+1}[n(n + 1)] + d_{n+1}[2n + 1] \\ &\quad = -c_n[n(2n - 1)/\hat{c}] - d_n(4n - 1)/\hat{c} \\ &\qquad - c_{n-1}[\gamma - K + (n - 1)^2]/\hat{c}^2 \\ &\qquad - d_{n-1}2(n - 1) - c_{n-2}\delta\gamma/\hat{c}^3 - a_{n-1}\delta\gamma/\hat{c}^2 \\ &d_{n+1}[n(n + 1)] = -d_n[n(2n - 1)/\hat{c}] \\ &\qquad - d_{n-1}[\gamma - K + (n - 1)^2]/\hat{c}^2 \\ &\qquad\quad - d_{n-2}\delta\gamma/\hat{c}^3 - b_{n-1}\delta\gamma/\hat{c}^2 \end{aligned}\right\}, \tag{A18}$$

for $n - 2, \ldots, N_0 - 1$. The starting values for the recursion relations (A18) are given in the following table:

j	a_0	a_1	a_2	b_1	b_2	c_0	c_1	c_2	d_1	d_2
1	0	1	0	0	0	0	0	0	0	0
2	0	0	$-\gamma/2\hat{c}^2$	0	0	1	0	$(K - \gamma)/2\hat{c}^2$	0	0
3	0	0	0	0	0	0	1	$-1/2\hat{c}$	0	0
5	1	0	$(K - 2)/2\hat{c}^2$	$1/\hat{c}$	0	0	0	$-\delta\gamma/2\hat{c}^2$	0	0

Notice that for $j = 1$, 2 and 3 the logarithmic terms in (A17) are entirely absent, while for $j = 4$, they begin with b_1 and d_3 nonzero in the upper and lower layer solutions respectively.

For symmetric modes in a double gyre (cf. Section 4), the boundary conditions (41) require different targets for the shooting method. For the solutions to (34), iterate in $\hat{c}$ until

$$\sqrt{K}Z(\xi_{N+1}) + (\hat{c} - 1)^{-1}Y(\xi_{N+1}) = 0; \tag{A19}$$

for the solutions to (38), on the other hand, the targets are

$$(\hat{c} - 1)^{-1}y_1(\xi_{N+1}) = y_2(\xi_{N+1}) = 0. \tag{A20}$$

Finite-element numerical techniques were used in obtaining closed basin solutions to Eqs. (12) and (13). In this method each of the dependent variables is represented as a series of basis functions; e.g.,

$$\psi_1(x,y) = \sum_n a_n\phi_n(x,y). \tag{A21}$$

For our square geometry, a separable set of basis functions were used, i.e.,

$$\phi_n(x,y) = s(x,x_n)s(y,y_n), \tag{A22}$$

where the $s(x,x_n)$ is a cubic B spline centered about the point x_n (Hirsh, 1975). Eqs. (12) and (13) were solved in forms obtained by multiplying them by ϕ_m and integrating over the basin. Thus transformed, the steady equation (12) was solved iteratively until convergence. Eq. (13) was solved as a matrix eigenvalue problem for the eigenfrequencies ω.

The cubic B spline $s(x,x_n)$ is nonzero over an interval of $4h$ centered about a node point x_n, where h is the interval between node points. The maximum resolution available for the calculations of Section 6 permitted 14 node points in each of the x and y directions (which corresponds to an h of 1/11 of the domain width). Because these basis functions are cubic polynomials, one may crudely identify their resolution capabilities with those of three times as many linear basis functions (such as second-order finite differences).

REFERENCES

Benney, D. J., and R. F. Bergeron, 1969: A new class of nonlinear waves in parallel flows. *Stud. Appl. Math.*, **48**, 181–204.

Drazin, P., and L. Howard, 1966: Hydrodynamic stability of parallel flow of inviscid fluid. *Advances in Applied Mechanics*, Vol. 9, Academic Press, **9**, 1–89.

Fofonoff, N. P., 1954: Steady flow in a frictionless homogeneous ocean. *J. Mar. Res.*, **13**, 254–262.

Haidvogel, D. B., and W. R. Holland, 1978: The stability of ocean currents in eddy-resolving general circulation models. *J. Phys. Oceanogr.*, **8**, 393–413.

Hansen, D., 1970: Gulf Stream meanders between Cape Hatteras and the Grand Banks. *Deep-Sea Res.*, **17**, 495–511.

Hirsh, J., 1975: The finite element method applied to ocean circulation problems. *Numerical Models of Ocean Circulation*, Nat. Acad. Sci., Washington, D. C., 363 pp.

Lin, C. C., 1966: *The Theory of Hydrodynamic Stability*. Cambridge University Press, 155 pp.

Luyten, J., 1977: Scales of motion in the deep Gulf Stream and across the continental rise. *J. Mar. Res.*, **35**, 49–74.

McWilliams, J. C., 1977a: On a class of stable, slightly geostrophic mean gyres. *Dyn. Atmos. Oceans*, **2**, 19–28.

——, 1977b: A note on a consistent quasigeostrophic model in a multiply-connected domain. *Dyn. Atmos. Oceans*, **1**, 427–441.

——, W. R. Holland and J. H. S. Chow, 1977: A description of numerical Antarctic Circumpolar Currents. *Dyn. Atmos. Oceans*, (in press).

Orlanski, I., and M. Cox, 1973: Baroclinic instability in ocean currents. *Geophys. Fluid Dyn.*, **4**, 297–332.

Pedlosky, J., 1964: The stability of currents in the atmosphere and ocean. Part I. *J. Atmos. Sci.*, **21**, 201–219.

Rhines, P., 1970: Edge-, bottom-, and Rossby waves in a rotating, stratified fluid. *Geophys. Fluid Dyn.*, **1**, 283–302.

Robinson, A., J. Luyten, and F. Fuglister, 1974: Transient Gulf Stream meandering. Part I: An observational experiment. *J. Phys. Oceanogr.*, **4**, 237–255.

Schmitz, W., 1976: Eddy kinetic energy in the deep western North Atlantic. *J. Geophys. Res.*, **81**, 4981–4982.

Veronis, G., and H. Stommel, 1956: The action of a variable wind stress on a stratified ocean. *J. Mar. Res.*, **15**, 43–75.